

Generalized Variational Mode Decomposition: A Multiscale and Fixed-Frequency Decomposition Algorithm

Yanfei Guo^{ID} and Zhousuo Zhang^{ID}

Abstract—To overcome the limitations of variational mode decomposition (VMD) algorithm that its frequency scales and spectrum positions cannot be flexibly adjusted to decompose signals as required, a generalized VMD (GVMD) was proposed. This article addresses the fundamental theory of GVMD. In order to highlight the local characteristics of the signal much more while considering its global data fidelity, a set of variational models is formed, where individual constrained optimization problem is constructed for each mode. The formed variational models are solved by the modified alternating direction method of multipliers approach, thus realizing the multiscale and fixed-frequency decomposition. To gain a deep insight into GVMD algorithm, its frequency band division manner is investigated. In essence, GVMD can be viewed as a bank of filters whose bandwidths and center frequencies can be flexibly adjusted by its parameters, i.e., scale parameters and prior center frequencies. The effectiveness of GVMD is verified on simulated and real signals. The preliminary results show that compared with state-of-the-art methods, GVMD can make full use of feature information to decompose original signals as desired into several narrowband modes or into several narrowband modes and a wideband mode, effectively obtaining the interested modes.

Index Terms—Chirp mode decomposition, empirical mode decomposition (EMD), frequency band division, multiscale and fixed-frequency decomposition, variational mode decomposition (VMD), wavelet packet transform (WPT).

I. INTRODUCTION

VARIATIONAL mode decomposition (VMD) was proposed by Dragomiretskiy and Dominique [1] in 2014, which adaptively and nonrecursively decomposes the signal into a series of principal narrowband modes (called variational mode functions, VMFs) while obtaining their center frequencies. Compared with the popular methods, such as

Manuscript received February 9, 2021; revised March 27, 2021; accepted April 14, 2021. Date of publication April 29, 2021; date of current version May 13, 2021. This work was supported in part by the Science Challenge Project under Grant TZ2018007, in part by the National Natural Science Foundation of China under Grant 51775410, in part by the Shanxi Province Natural Science Foundation under Grant 201801D121129, and in part by the Shanxi Province Key Research and Development Project under Grant 201903D121137. The Associate Editor coordinating the review process was Qiang Miao. (*Corresponding author: Yanfei Guo*)

Yanfei Guo is with the School of Electronics and Information Engineering, Taiyuan University of Science and Technology, Taiyuan 030024, China (e-mail: guoyanfei@tyust.edu.cn).

Zhousuo Zhang is with the School of Mechanical Engineering, Xi'an Jiaotong University, Xi'an 710049, China, and also with the State Key Laboratory for Manufacturing Systems Engineering, Xi'an Jiaotong University, Xi'an 710049, China (e-mail: zzs@xjtu.edu.cn).

Digital Object Identifier 10.1109/TIM.2021.3076569

wavelet transform (WT), wavelet packet transform (WPT), and empirical wavelet transform (EWT) [2], VMD is adaptive in basis function selection and frequency band division. VMD can be viewed as a data-driven method like empirical mode decomposition (EMD) [3] or its extended versions [4], [5]. Instead, it is necessary for WT, WPT, and EWT to select basis functions before decomposing signals. Therefore, their decomposition effect heavily depends on the shapes of basis functions. On the other hand, the signal decomposition process of most signal processing methods is accompanied by the frequency band division process. Reasonable frequency band segmentation is the key to the successful signal decomposition. The frequency band is divided in a regular fashion by WT and WPT [6]. For the EWT method, the frequency band segmentation is a prerequisite step to decompose signals. However, it is difficult for EWT to properly detect the spectrum support for all modes (i.e., weak modes) to reasonably segment the signal frequency band [6], [7]. EMD and its extended versions adaptively segment the frequency band [8]. Unfortunately, the frequency band is often divided improperly by the EMD-based methods, frequently resulting in mode mixing. As an alternative of EMD, VMD adaptively divides the frequency band through determining spectrum positions (via center frequencies) and frequency scales (or bandwidths). Recently, VMD has won some successes in multicomponent signal decomposition [9]–[11], weak feature extraction [12], [13], and denoising [14], [15].

However, several limitations of VMD have been found in practice because the frequency band cannot be divided properly or as required to obtain interested modes. First, multiple frequency scales of VMD cannot be adjusted flexibly. The frequency scales of VMD are proved to be related to the scale parameter to some extent, and a set of smaller frequency scales can be obtained with a larger scale parameter, and vice versa [16]–[20]. Unfortunately, the same scale parameter is employed to optimize all VMFs by VMD, which is not conducive to accurately capturing modes with different bandwidths. Second, the decomposition spectrum positions of VMD cannot be flexibly specified except for zero frequency. In engineering applications, real signals are often expected to be decomposed into the modes containing the feature information, such as gear failure frequencies, bearings feature frequencies, or the known interference frequencies, to further extract feature modes or remove noise contents. In particular, when the feature component is relatively weak,

it may be removed as noise or still submerged in other strong components since VMD obtains principal VMFs preferentially [21], [22]. Mohan *et al.* [23] proposed an improved VMD algorithm, which used frequency information to extract weak modes. However, the frequency scales of VMD were not taken into consideration. Third, VMD cannot identify the wideband mode with rapidly varying amplitude as one mode. The mode of VMD should be narrowband and well separate in the frequency domain. To overcome the shortcoming of VMD in analyzing crossed modes which are overlapped in the frequency domain but separate in the time-frequency domain, Chen *et al.* [24] presented a variational nonlinear chirp mode decomposition (VNCMD) to analyzing nonlinear chirp signals through using demodulation techniques and minimizing the bandwidth of the demodulated baseband signal. But it still imposes the same bandwidth parameter to optimize all modes and needs the accurate mode number to decompose signals. To overcome the shortcomings of VNCMD, Chen *et al.* [25] recently proposed an adaptive chirp mode pursuit (ACMP) to decompose the chirp signal to iteratively capture signal modes and employed it to effectively detect the rub-impact fault for rotor-stator system [26]. The VNCMD and ACMP methods can be viewed as improved VMD methods to analyze chirp signals through using demodulation techniques. However, if the original signal contains the wideband mode with rapidly varying instantaneous amplitude, such as the typical impulse content or impact vibration content in engineering, which can be considered to be the summing of lots of harmonic modes, these two methods cannot demodulate this kind of signals anymore. Finally, like most methods, VMD cannot decompose signals as required. In application, not all modes but part modes are expected to be separated from the original signal. That is, the original need not be decomposed into all constituent modes but into several modes to obtain interested modes since the mode number of the signal is a little difficult to determine in advance. And the feature information of interested modes, such as peak frequencies and bandwidth information, is usually available. Most signal processing methods usually use the prior information to select feature components or to remove interference during postprocessing. But these methods cannot directly employ feature information to decompose signals as required. To address the limitations stated above, a new generalized VMD (GVMD) algorithm was proposed to detect the interlayer slipping fault of viscoelastic sandwich cylindrical structure [22]. However, the algorithm model of GVMD is not yet involved, and the interpretation to GVMD is also not insightful.

The aim of this article is to establish the underlying mathematical model for GVMD, to shed light on its frequency band division manner, as well as to verify its effectiveness in making use of feature information to decompose signals as required to obtain interested results. The rest of this article is organized as follows. Section II completes the mathematical theory of GVMD and studies its frequency band division manner. The effectiveness of GVMD is verified through analyzing simulated and real signals in Section III. Finally, conclusions are given in Section IV.

II. PROPOSED ALGORITHM

A. Algorithm Model

To realize the multiscale and fixed-frequency decomposition, the underlying algorithm model of GVMD is proposed. In order to realize the multiscale decomposition, the proposed model constructs an individual variational model for each component. To realize the fixed-frequency decomposition, the proposed model is solved by the modified alternating direction method of multipliers (ADMM).

1) *Constructions of Constrained Optimization Problems:* Suppose that the signal x consists of K subsignals, i.e., $x = \sum_{k=1}^K x_k$, which are not overlapped in the frequency domain. In order to fully highlight the local characteristics of the signal, we apply the original VMD model to each subsignal x_k . A total of K constrained optimization problems are formulated as follows:

$$\begin{aligned} & \min_{u_k, \omega_k} \left\{ \left\| \partial_t \left[\left(\delta(t) + \frac{j}{\pi t} \right)^* u_k(t) \right] e^{-j\omega_k t} \right\|_2^2 \right\}, \quad (k=1, 2, \dots, K) \\ & \text{s.t. } u_k(t) = x_k(t) \end{aligned} \quad (1)$$

where u_k and ω_k are the k th VMF and its center frequency, respectively, δ is the Dirac distribution, t denotes time, $\|\cdot\|_2^2$ is the squared l_2 -norm, $*$ denotes the convolution, and $\partial_t(\cdot)$ denotes the partial gradient to time.

Although the local characteristics of the original signal is emphasized by problems (1), there is a fatal flaw. The measured signal is not the subsignals $x_k (k = 1, 2, \dots, K)$ but the mixed signal x . Therefore, problems (1) are unsolvable. The constrained functions in problems (1) should be modified. Each constrained subproblem is constructed for the VMF u_k based on the assumption that the others VMFs were known. Finally, the improved constrained optimization problems are formed as shown in the following problems:

$$\begin{aligned} & \min_{u_k, \omega_k} \left\{ \left\| \partial_t \left[\left(\delta(t) + \frac{j}{\pi t} \right)^* u_k(t) \right] e^{-j\omega_k t} \right\|_2^2 \right\}, \quad (k=1, 2, \dots, K) \\ & \text{s.t. } \sum_{k=1}^K u_k(t) = x(t). \end{aligned} \quad (2)$$

In problems (2), each objective function is the bandwidth of each VMF, embodying the local property of the algorithm; each constraint function is to reconstruct the original signal by all VMFs together so that VMFs are not isolated but dependent on one another, reflecting the global data fidelity of the algorithm. Therefore, GVMD can highlight the local characteristics of the signal much more while considering its global data fidelity. On the contrary, it is dilemmatic for VMD to well take both the local characteristics of the signal and its global data fidelity into consideration because only one constraint optimization problem is constructed for all VMFs.

2) *Solutions of Constrained Optimization Problems:* The multiplier method is introduced to convert each subproblem in problems (1) into an unconstrained optimization subproblem.

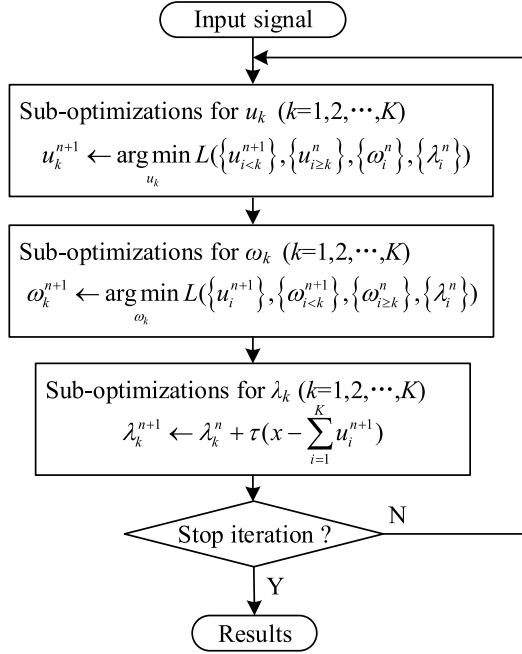


Fig. 1. Flowchart of solving problems (3) by ADMM.

The augmented Lagrangian functions are expressed as follows:

$$\begin{aligned} L(u_k, \omega_k, \lambda_k) &:= \alpha_k \left\| \partial_t \left[\left(\delta(t) + \frac{j}{\pi t} \right)^* u_k(t) \right] e^{-j\omega_k t} \right\|_2^2 \\ &\quad + \left\langle \lambda_k(t), x(t) - \sum_k u_k(t) \right\rangle + \left\| x(t) - \sum_k u_k(t) \right\|_2^2 \\ (k = 1, 2, \dots, K) \end{aligned} \quad (3)$$

where α_k is the scale parameter and $\lambda_k(t)$ is the Lagrangian multiplier.

Since each subproblem in problems (2) is constructed based on the assumption that the other VMFs were known, any unconstrained subproblem in problems (3) cannot be solved in an independent way. On the other hand, ADMM is well suited to deal with the distributed convex optimization [27]. It takes the form of a decomposition-coordination procedure in which the solutions to small local subproblems are coordinated to a solution to a large global problem. So, ADMM is suited to address unconstrained problems (3) which can be conveniently divided into three types of subproblems, i.e., the suboptimizations of augmented Lagrangian functions with regard to u_k , ω_k , and λ_k , respectively. The flowchart of solving problems (3) by ADMM is shown in Fig. 1. And the saddle points are the solutions to problems (2).

From problems (3), it can be seen that personalized scale parameters rather than the same scale parameter can be set for all VMFs, realizing to flexibly adjust frequency scales of GVMD. However, in engineering part or all of VMFs are often expected to be located around certain spectrum positions. It is necessary to design a smart scheme to achieve the fixed-frequency decomposition. During the process of the unconstrained optimization problems (3) solved by ADMM

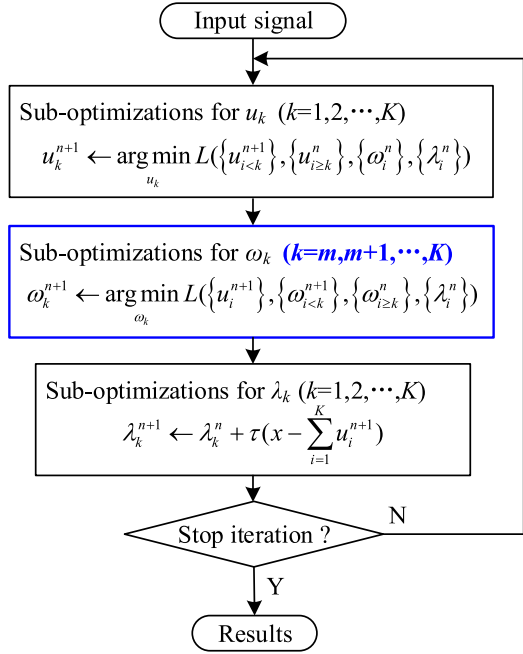


Fig. 2. Flowchart of solving problems (3) by improved ADMM.

shown in Fig. 1, the VMFs $u_k(k = 1, 2, \dots, K)$ and their center frequencies $\omega_k(k = 1, 2, \dots, K)$ are updated iteratively. Therefore, once $m(0 \leq m \leq K)$ center frequencies of VMFs were *a priori*, the prior center frequencies $\omega_k(k = 1, 2, \dots, m)$ should not be updated anymore, and the VMFs $u_k(k = 1, 2, \dots, m)$ could be optimized accurately and quickly around these known center frequencies, thus realizing the fixed-frequency decomposition. And the other $K-m$ VMFs and their center frequencies are still optimized adaptively by the algorithm. To this end, an improved ADMM is formed to solve problems (3), whose flowchart is shown as Fig. 2.

Naturally, the suboptimizations of each augmented Lagrangian function shown in problems (3) with regard to u_k , ω_k , and λ_k can be expressed as the following equivalent suboptimization problems, respectively:

$$\begin{aligned} u_k^{n+1} &= \arg \min_{u_k \in X} \left\{ \alpha_k \left\| \partial_t \left[\left(\delta(t) + \frac{j}{\pi t} \right)^* u_k(t) \right] e^{-j\omega_k t} \right\|_2^2 \right. \\ &\quad \left. + \left\| x(t) - \sum_{i=1}^K u_i(t) + \frac{\lambda_k(t)}{2} \right\|_2^2 \right\} \end{aligned} \quad (4)$$

$$\omega_k^{n+1} = \arg \min_{\omega_k} \left\{ \alpha_k \left\| \partial_t \left[\left(\delta(t) + \frac{j}{\pi t} \right)^* u_k(t) \right] e^{-j\omega_k t} \right\|_2^2 \right\} \quad (5)$$

$$\lambda_k^{n+1} \leftarrow \lambda_k^n + \tau \left(x - \sum_{i=1}^K u_i^{n+1} \right) \quad (6)$$

where τ is the step size of the Lagrangian multiplier to iteratively update itself.

The remaining solving details are the same as those in VMD. To keep this article largely self-contained, the details are given as follows:

a) *Minimization for u_k :* The Parseval/Plancherel Fourier isometry under l_2 -norm is used to solve the problems in the

frequency domain. Equation (4) can be expressed as follows:

$$\hat{u}_k^{n+1} = \arg \min_{\hat{u}_k, u_k \in X} \left\{ \alpha_k \|j\omega(1 + \text{sgn}(\omega + \omega_k))\hat{u}_k(\omega + \omega_k)\|_2^2 + \left\| \hat{x}(\omega) - \sum_{i=1}^K \hat{u}_i(\omega) + \frac{\hat{\lambda}_k(\omega)}{2} \right\|_2^2 \right\}. \quad (7)$$

By performing a change of variables for the first term on the right-hand side of (7), (7) can be expressed as follows:

$$\hat{u}_k^{n+1} = \arg \min_{\hat{u}_k, u_k \in X} \left\{ \alpha_k \|j(\omega - \omega_k)[(1 + \text{sgn}(\omega))\hat{u}_k^n(\omega)]\|_2^2 + \left\| \hat{x}(\omega) - \sum_{i=1}^K \hat{u}_i(\omega) + \frac{\hat{\lambda}_k(\omega)}{2} \right\|_2^2 \right\}. \quad (8)$$

By using the Hermitian symmetry of the real signals in the reconstruction fidelity term, (8) can be rewritten as follows:

$$\hat{u}_k^{n+1} = \arg \min_{\hat{u}_k, u_k \in X} \left\{ \int_0^\infty 4\alpha_k(\omega - \omega_k)^2 |\hat{u}_k^n(\omega)|^2 + 2 \left| \hat{x}(\omega) - \sum_{i=1}^K \hat{u}_i(\omega) + \frac{\hat{\lambda}_k(\omega)}{2} \right|^2 d\omega \right\}. \quad (9)$$

By using Euler equation of the variational method, the solution of (9) can be found as follows:

$$\hat{u}_k^{n+1}(\omega) = \frac{\hat{x}(\omega) - \sum_{i \neq k} \hat{u}_i(\omega) + \frac{\hat{\lambda}_k(\omega)}{2}}{1 + 2\alpha_k(\omega - \omega_k)^2}. \quad (10)$$

The VMF in the time domain is obtained as the real part of the inverse Fourier transformation of (10).

b) *Minimization for ω_k* : Similarly, the minimization of each augmented Lagrangian function shown in subproblems (5) with respect to ω_k can be expressed as follows:

$$\omega_k^{n+1} = \arg \min_{\omega_k} \left\{ \alpha_k \left\| \partial_t \left[\left(\delta(t) + \frac{j}{\pi t} \right)^* u_k(t) \right] e^{-j\omega_k t} \right\|_2^2 \right\}. \quad (11)$$

Let us solve the problems in the frequency domain as before. Equation (11) can be rewritten as follows:

$$\omega_k^{n+1} = \arg \min_{\omega_k} \left\{ \int_0^\infty (\omega - \omega_k)^2 |\hat{u}_k^n(\omega)|^2 d\omega \right\}. \quad (12)$$

The solution is found as follows:

$$\omega_k^{n+1} = \frac{\int_0^\infty \omega |\hat{u}_k(\omega)|^2 d\omega}{\int_0^\infty |\hat{u}_k(\omega)|^2 d\omega}. \quad (13)$$

From the previous derivation, it can be seen that the mathematical theory on constructions and solutions of constrained optimization problems is rigorous. Like VMD, GVMD is adaptive and nonrecursive, and the resulting VMFs can reconstruct the input signal either exactly or in a least-squares sense. In this article, the latter reconstructed manner is adopted.

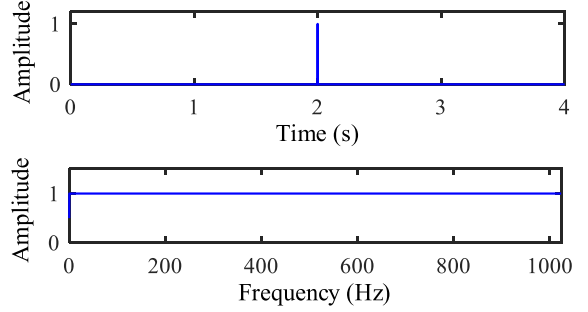


Fig. 3. Dirac pulse. The first row is the waveform and the second row is the normalized amplitude spectrum.

However, unlike VMD, GVMD can highlight the local characteristics of the signal more while considering its global data fidelity, and has the property of the multiscale and fixed-frequency decomposition. Personalized scale parameter can be flexibly adjusted to extract each mode according to its bandwidth information, and the center frequencies can be fixed to extract part or all modes in the expected spectral positions. Once all scale parameters are identical and no prior center frequency is specified, GVMD is the same as VMD. That is, VMD can be looked on as a special case of GVMD. To sum up, GVMD can use feature information to decompose the original signal as required into several narrowband modes or several narrowband modes and a wideband mode owing to the property of the multiscale and fixed-frequency decomposition. It is worth noting that GVMD also decomposes signals in the frequency domain. The modes can be close even interlaced but not be overlapped in the frequency domain.

B. Frequency Band Division Manner

The frequency band division is an important part for most signal decomposition methods. The frequency band divisions of WT and WPT are in a regular manner regardless of the frequency distribution of the signal. The frequency band divisions of the EMD-based methods and VMD are both signal-dependent. However, mode mixing always occurs due to the unreasonable frequency band divisions of these methods. Unlike most signal decomposition methods, GVMD can segment the frequency band as required. To gain a deep insight into the nature of the frequency band division of GVMD, a Dirac pulse with uniform spectrum distribution is analyzed.

Here, the frequency scales and spectrum positions of GVMD are separately expressed in terms of the bandwidths and center frequencies of impulse response modes. In order to illustrate the frequency band division manner, assume that the Dirac pulse shown in Fig. 3 would be decomposed by GVMD with different bandwidths at different spectrum positions. A total of four situations are designed, as shown in Figs. 4–7. In Fig. 4, the whole frequency band is finely divided into five segments, where five VMFs are located around the spectrum positions specified by prior center frequencies, and their bandwidths are negatively correlated with scale parameters. In Fig. 5, the low-frequency band is divided relatively finely, where VMF1–VMF4 are optimized around

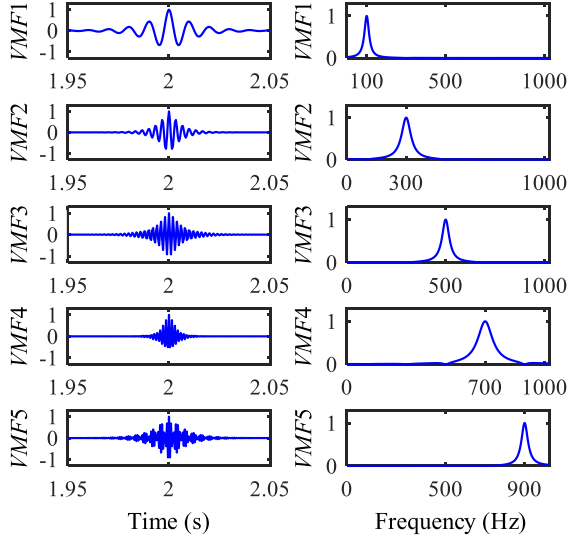


Fig. 4. Normalized VMFs of GVMD with $f = [100, 300, 500, 700, 900]$ Hz, $\alpha = [20000, 5000, 8000, 2000, 10000]$, $K = 5$, and $m = 5$. The left column is the normalized waveforms, and the right column is the normalized amplitude spectrums. The whole frequency band is divided as needed.

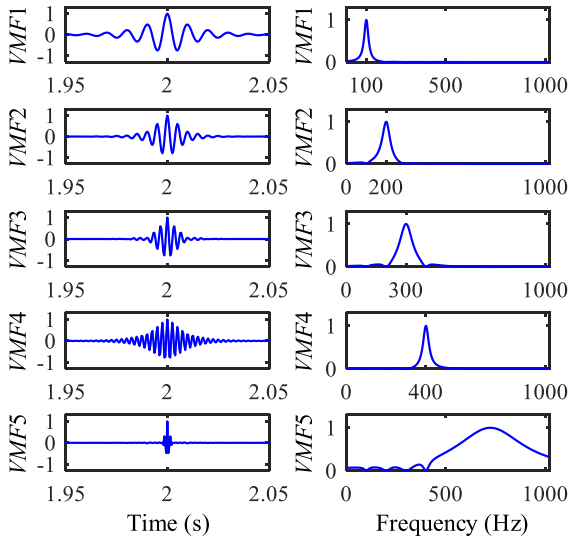


Fig. 5. Normalized VMFs of GVMD with $f = [100, 200, 300, 400, 0]$ Hz, $\alpha = [20000, 5000, 2000, 8000, 100]$, $K = 5$, and $m = 4$. The left column is the normalized waveforms and the right column is the normalized amplitude spectrums. The low-frequency band is divided relatively finely, and the high-frequency band is segmented relatively coarsely.

the specified spectrum positions with smaller frequency scales. The high-frequency band is segmented relatively coarsely, where VMF5 is adaptively obtained owing to the property of the global data fidelity. Contrary to the scenarios in Fig. 5, the high-frequency band is divided finely in Fig. 6, where VMF1–VMF4 are optimized around the specified spectrum positions with smaller frequency scales. The low-frequency band is segmented relatively coarsely, where VMF5 is adaptively obtained owing to the property of the global data fidelity. In Fig. 7, the medium-frequency band is divided locally and finely, where VMF1 and VMF2 are optimized around the specified frequency positions with smaller frequency scales.

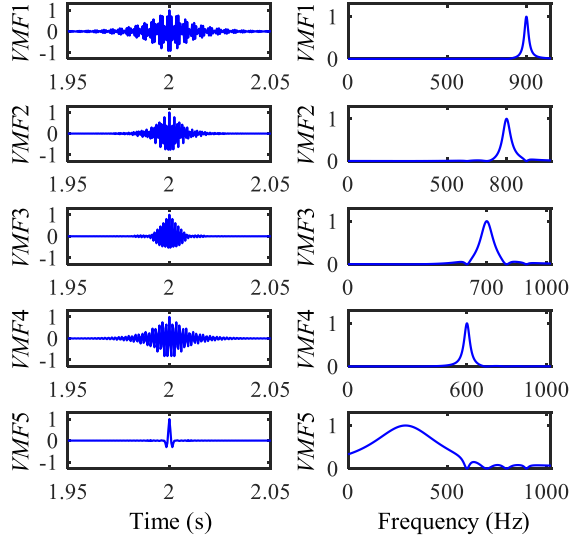


Fig. 6. Normalized VMFs of GVMD with $f = [900, 800, 700, 600, 0]$ Hz, $\alpha = [20000, 5000, 2000, 8000, 100]$, $K = 5$, and $m = 4$. The left column is the normalized waveforms and the right column is the normalized amplitude spectrums. The high-frequency band is divided relatively finely, and the low-frequency band is segmented relatively coarsely.

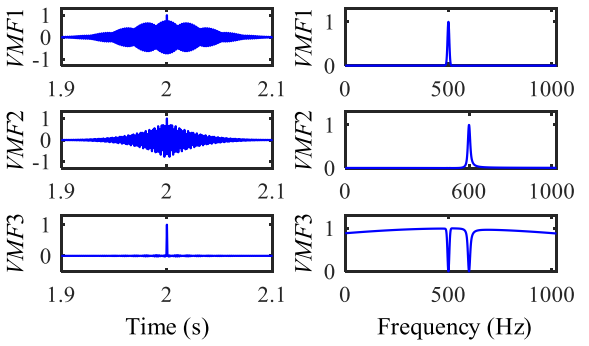


Fig. 7. Normalized VMFs by GVMD with $f = [500, 600, 0]$ Hz, $\alpha = [500, 500, 2]$, $K = 3$, and $m = 2$. The left column is the normalized waveforms and the right column is the normalized amplitude spectrums. The medium-frequency band is divided locally and finely, and the remaining frequency band is coarsely divided.

The remaining frequency band is divided coarsely, where VMF3 estimates the residual signal owing to the property of global data fidelity. It is interesting that VMF3 is interlaced with VMF1 and VMF2 in the frequency domain.

The above analysis indicates that unlike the existing methods such as WT, EMD, VMD, VNCMD, and ACMP, GVMD can flexibly divide the frequency band through adjusting its frequency scales and spectrum positions owing to the property of the multiscale and fixed frequency decomposition. The spectrum positions of part or all of VMFs are determined by prior center frequencies, and the frequency scales are influenced by the scale parameters. A smaller frequency scale decomposition will be realized by GVMD with a larger scale parameter in given situations. Therefore, it is expected that GVMD can decompose the original signal as required into several narrowband modes or into several narrowband modes and a wideband mode. However, the frequency bands covered

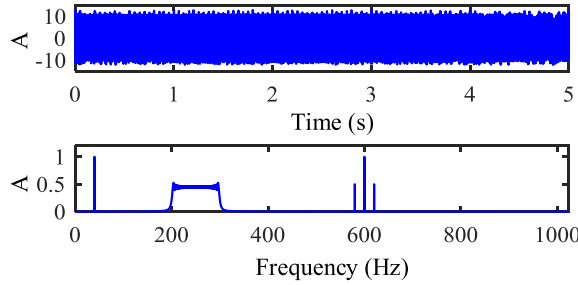


Fig. 8. Simulated signal. The first row is the waveform and the second row is the amplitude spectrum.

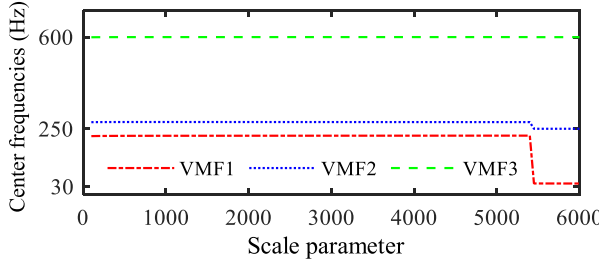


Fig. 9. Changes of center frequencies of VMFs with scale parameter. Red dash-dotted line: VMF1, blue dotted line: VMF2, and green dashed line: VMF3.

by the constituent modes may be close, even interlaced, but they must not be overlapped.

III. EXAMPLES AND DISCUSSION

Multicomponent signal decomposition and denoising are important tasks in structure health monitoring, fault diagnosis, and biomedical signal processing. In this section, simulated and real signals are analyzed by GVMD to verify its effectiveness in decomposing signals as required.

A. AM–FM Signal Separation

When the rotating machine is running with some faults or the structure state deteriorates, the feature information of the machine fault or structure state is often amplitude-modulated (AM) or frequency-modulated (FM). Therefore, it is necessary to extract the AM and FM modes. Here, the simulated signal, defined by the following equation, is composed of a harmonic mode s_1 , an FM mode s_2 , and an AM mode s_3 , as shown in Fig. 8. The sampling frequency is 2048 Hz, and the signal length is 5 s. The center frequencies of three constituent modes are 40, 250, and 600 Hz, respectively. The bandwidths of three modes are markedly different

$$\begin{cases} s_1 = \cos(80\pi t) \\ s_2 = 10 \cos(400\pi t^2 + 20\pi t) \\ s_3 = (1 + \cos(40\pi t)) \cos(1200\pi t) \\ s = s_1 + s_2 + s_3. \end{cases} \quad (14)$$

First, the simulated signal is processed by VMD. In order to obtain better decomposition effect, the mode number K is 3, and the scale parameter is optimized using the method

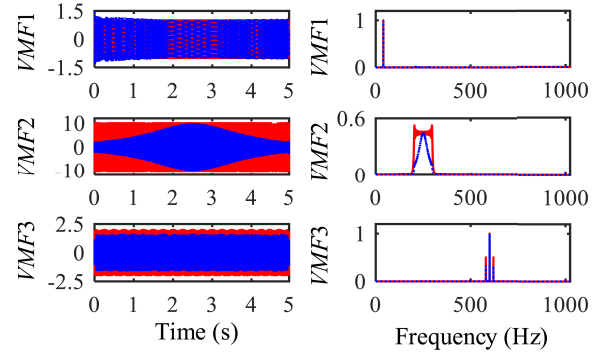


Fig. 10. VMFs of VMD with the optimized scale parameter. The left column is the waveforms and the right column is the amplitude spectrums. Red solid line: the original components and blue dotted line: VMFs. There is information loss in VMF2 and VMF3.

proposed in [17]. The center frequencies of VMFs are introduced to judge whether VMD captures the modes in the proper spectral positions or not. Fig. 9 gives the changes of center frequencies of VMFs obtained by VMD with the scale parameter varying from 100 to 6000. The results indicate when scale parameter is less than 5450, VMD cannot well capture the harmonic mode s_1 and the FM mode s_2 . When the scale parameter reaches 5450, the center frequencies of three VMFs are close to the theoretical values, respectively. That means VMD can capture VMFs in the proper spectrum positions. The optimized scale parameter is selected to be 5450 because a relatively smaller scale parameter can improve the data fidelity of VMD algorithm [1], [16], [17]. The results decomposed by VMD with the optimized scale parameter are shown in Fig. 10. Obviously, VMD with a larger scale parameter can well extract the narrowband harmonic mode, but some useful information is lost for the wideband AM and FM modes, which is caused due to the frequency scales of VMD being too small. However, VMD cannot capture the proper spectral positions for three modes with a smaller scale parameter.

Then, the original signal is decomposed by GVMD with prior center frequency information to achieve the fixed-frequency decomposition, but its scale parameters are set to be identical. The relative error defined by the following equation [1] is introduced to evaluate the estimated error of VMF to the original mode:

$$e(k) = \frac{\|s_k - u_k\|_2}{\|s_k\|_2} \quad (15)$$

where $\|\cdot\|_2$ denotes the l_2 -norm, s_k denotes the k th original mode, u_k denotes the k th VMF.

We perform the error analysis for GVMD with identical scale parameters varying from 10 to 20000. The results are shown in Fig. 11. The estimated errors of three original modes show different changing trends with the scale parameters. GVMD can gain smaller estimated error for the harmonic mode with a larger scale parameter, and gain smaller estimated error for the AM mode and the FM mode with smaller scale parameters. However, GVMD cannot accurately extract all modes with markedly different bandwidths because all scale parameters are selected to be identical.

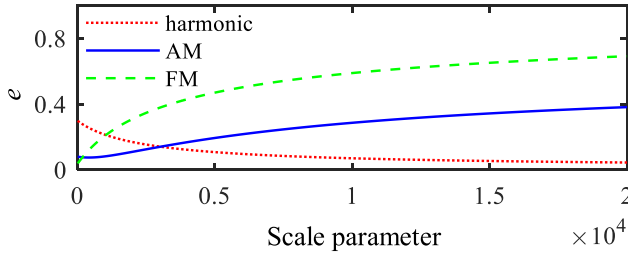


Fig. 11. Relative error of VMFs to the original components. The VMFs are obtained by GVMD with prior center frequencies and identical scale parameters.

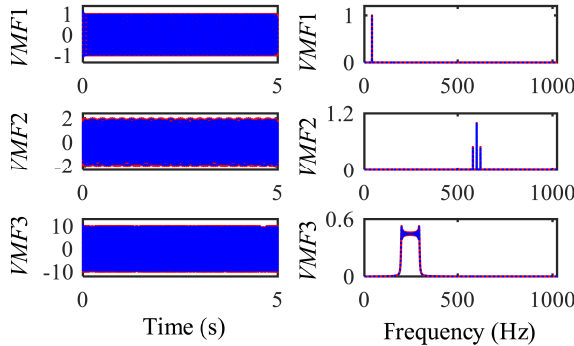


Fig. 12. VMFs of GVMD with two prior center frequencies and different scale parameters. The left column is the waveforms and the right column is the amplitude spectrums. Blue dotted line: VMFs and red solid line: the original components. All components are accurately extracted.

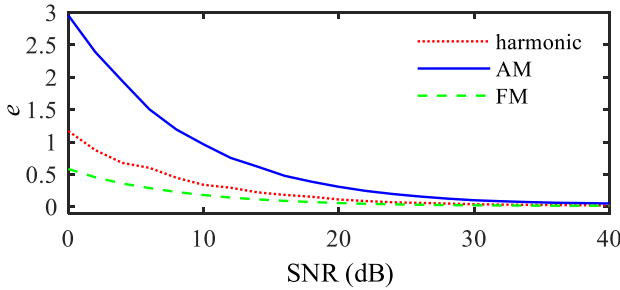


Fig. 13. Noise robustness analysis of GVMD.

Finally, three personalized scale parameters are set and the center frequencies of the harmonic mode and AM mode are specified. The results of GVMD with $K = 3$, $m = 2$, $\alpha = [20000, 300, 50]$, and $f = [40, 600, 0]$ Hz are shown in Fig. 12. The estimated errors of the harmonic mode, AM mode, and FM mode are 0.020, 0.042, and 0.015, respectively. The results indicate that three modes are accurately extracted by GVMD through flexibly adjusting the spectrum positions and frequency scales based on the signal itself.

In order to discuss the noise robustness of GVMD, Gaussian noise with mean value of 0 and variance value of 1 is added to the original signal. The signal-to-noise ratio (SNR) increases from 0 to 40 dB. The estimated error of three modes is shown in Fig. 13. It can be seen that the higher the SNR, the smaller the estimated errors of three original modes, the better the decomposition effect. When the SNR is larger than 30 dB, three estimated errors are less than 0.1 the decomposition effect is better. When the SNR is less than 10 dB, the estimated

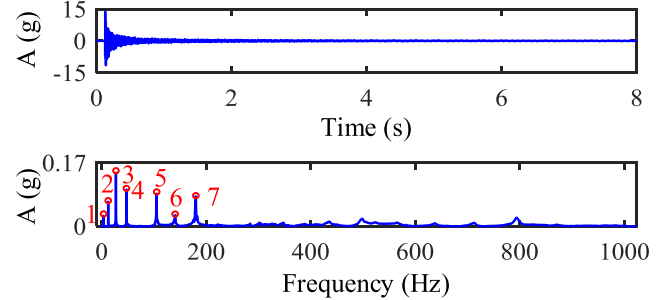


Fig. 14. Impulse response vibration signal. The first row is the waveform and the second row is the amplitude spectrum.

error of the AM mode is larger than 1, and the decomposition effect is relatively worse. The reason is that too much noise content is preserved due to a larger local frequency scale. Adjusting the scale parameters or considering the AM mode to be three harmonic modes may be a good idea. However, how to optimize the scale parameters of GVMD for the modes with different bandwidths is out of the scope of this work. In addition, if the modulation frequency of the AM mode is needed, the amplitude demodulation analysis should be conducted further.

B. Multicomponent Signal Decomposition

To verify the effectiveness of GVMD in multicomponent signal decomposition, the measured acceleration vibration signal of the explosive clad pipe is taken as an example. The explosive clad pipe welded by stainless steel and carbon steel under a high velocity collision formed by energy of explosives. The defect detection should be conducted to avoid leakage accidents before the explosive clad pipe enters the service. The feature information, which is often hidden in one or more constituent modes of the original vibration signal, should be extracted to effectively detect the bonding state. Fig. 14 gives the impulse response signal of the explosive clad pipe which is simply supported at two ends. The sampling frequency is 2048 Hz, and the data length is 8 s. More details about the experiments can be found in reported work [28]. As can be seen from Fig. 14 that the vibration signal mainly consists of seven narrowband vibration modes in the low frequency band, whose peak frequencies are 3.125, 12, 26.88, 47.13, 104.6, 140.4, and 179.6 Hz, respectively.

In order to extract vibration modes 1–7, seven prior center frequencies and relatively larger scale parameters are set for GVMD to finely divide the low-frequency band, and no prior center frequency and a relatively smaller scale parameter are set to coarsely divide the high-frequency band. The results of GVMD with, $\alpha = [1000, 1000, 1000, 1000, 800, 800, 100]$, $f = [3.125, 12, 26.88, 47.13, 104.6, 140.4, 179.6, 0]$ Hz, $K = 8$, and $m = 7$ are shown in Fig. 15. Interested vibration modes 1–7 are well estimated by VMF1–VMF7, respectively. And the residual signal is estimated by VMF8, which is identified as a wideband mode. The results indicate that GVMD can decompose the multicomponent signal as required into multiple interested modes owing to the property of multiscale and fixed-frequency decomposition, which is

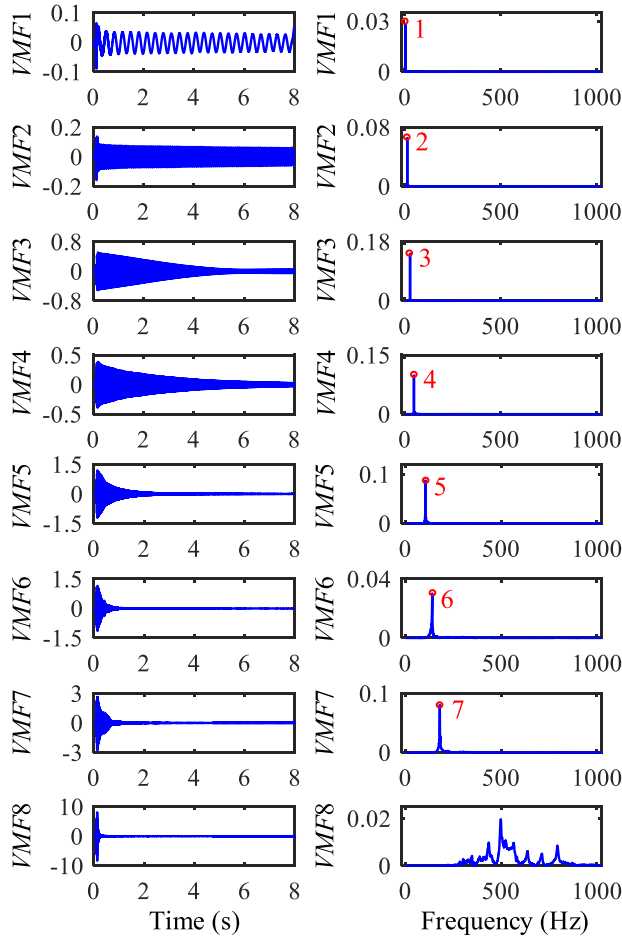


Fig. 15. Results decomposed by GVMD. The left column is the waveforms and the right column is the amplitude spectrums. Seven interested vibration modes are extracted as required.

expected to provide more information for finding out the sensitive modes to the bonding state.

As a contrast, VMD is used to analyze the original signal. Fig. 16 provides the results of VMD with $\alpha = 7000$ and $K = 8$. The desired vibration modes 3–7 are well estimated by VMF2, VMF3, VMF4, VMF6, and VMF7, respectively. However, relatively weak and close vibration mode 1 and mode 2 are still blended in VMF1. VMF5 and VMF8 are uninterested frequency contents.

The original signal is again decomposed by WPT with the Daubechies wavelet function of “db9” and the decomposition level of 7. Based on the WPT theory, vibration modes 1–7 are expected to be located in the 1st, 2nd, 4th, 6th, 14th, 18th, and 23rd subbands, respectively. The reconstructed results of WPT are shown in Fig. 17. Interested vibration modes 1–7 are estimated by s_1 – s_7 , respectively, and the residual signal is estimated by s_8 . Obviously, interested vibration modes 2–7 are corrupted by neighboring frequency contents owing to the energy leak of WPT.

C. Denoising

The measured signals are often corrupted by various interferences. Denoising can highlight the feature information. In the following, the ECG record file 101 from the MIT-BIH

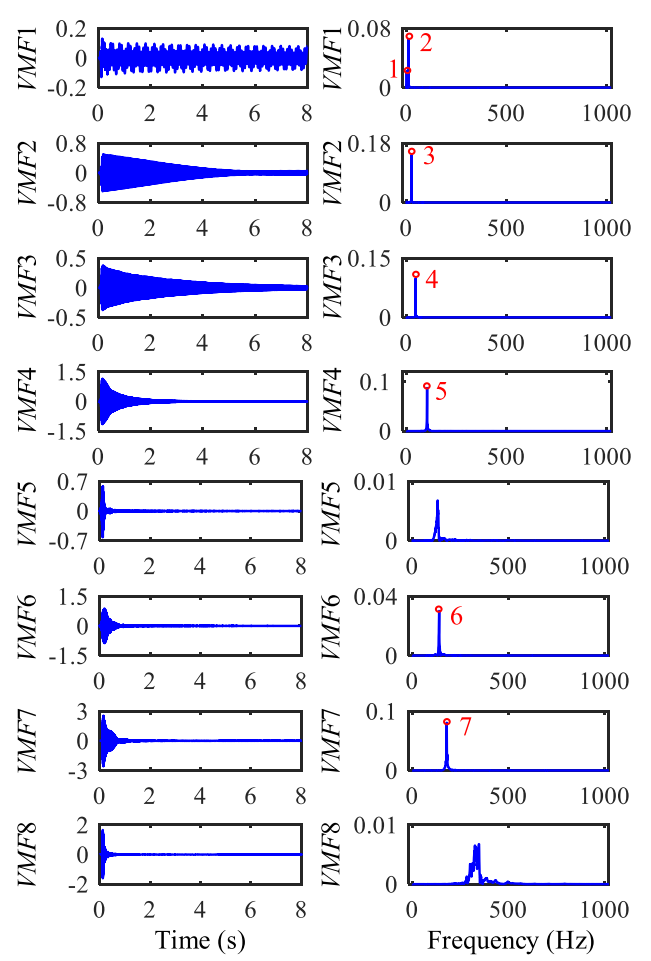


Fig. 16. Results of VMD. The left column is the waveforms and the right column is the amplitude spectrums. Only parts of interested vibration modes are extracted, and mode mixing occurs.

Arrhythmia database shown in Fig. 18 is an example [29]. The sampling frequency is 360 Hz and the data length is 30 s. It is obvious that the ECG signal is corrupted by the strong low-frequency trend and the weak 60 Hz power line interference.

Two noise terms are narrowband and their peak frequencies are available. The clean ECG can be considered as a wideband mode. To effectively remove the noise terms, prior center frequencies and larger scale parameters are set to finely divide the local frequency bands, and no prior center frequency and a relatively smaller scale parameter are set to coarsely divide the residual frequency band. Fig. 19 provides the results of GVMD with $K = 3$, $m = 2$, $\alpha = [10^4, 10^6, 10]$, and $\omega = [0, 60, 0]$ Hz. The strong low-frequency trend and the weak 60 Hz power line interference are separated from the original signal by GVMD using smaller frequency scale and fixed-frequency decomposition, which are well estimated by VMF1 and VMF2. The clean ECG with rapidly varying amplitude is adaptively identified as a wideband mode by GVMD using the property of global data fidelity, which is estimated by VMF3. Two resulted noise terms are affected less by adjacent frequency contents. In other words, more useful information may be retained by the denoised ECG.

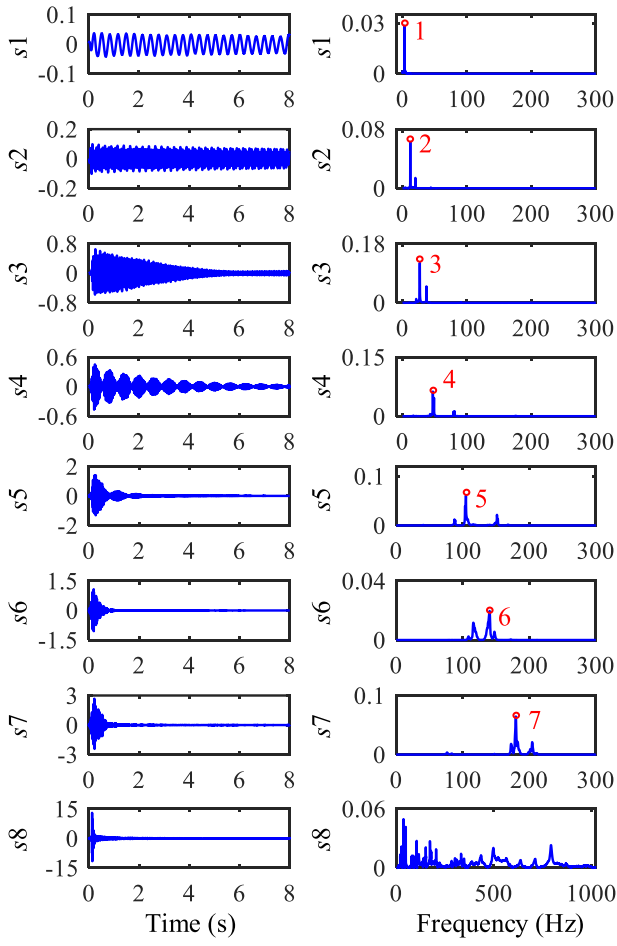


Fig. 17. Results reconstructed by WPT. The left column is the waveforms and the right column is the amplitude spectrums. Interested vibration modes 2–7 are corrupted by neighboring frequency contents owing to the energy leak of WPT.

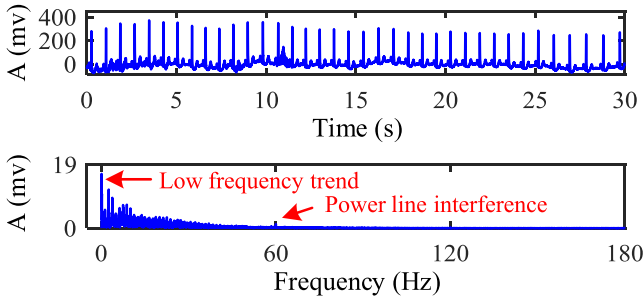


Fig. 18. Noisy ECG. The first row is the waveform and the second row is the amplitude spectrum.

When the original ECG signal is decomposed by the methods such as VMD, complementary ensembled EMD (CEEMD), and WPT, it must be decomposed into numerous modes by these methods first, then the clean ECG signal can be reconstructed after post-processing. To save space, the decomposed results by these methods are omitted, and only the reconstructed results are provided in the following.

The reconstructed results of VMD with $\alpha = 1000$ and $K = 10$ are shown in Fig. 20. The low-frequency trend, the

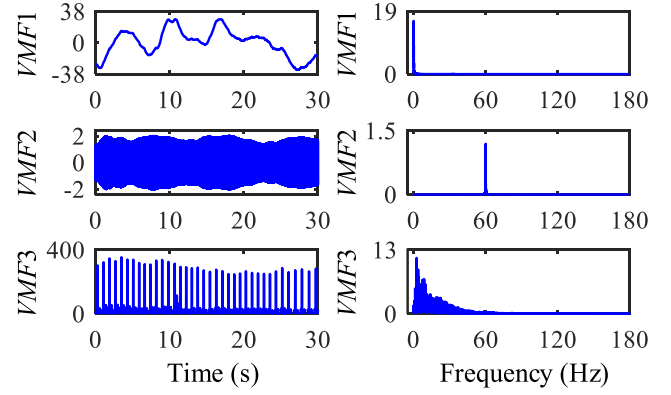


Fig. 19. Results of GVMD. The left column is the waveforms, and the right column is the amplitude spectrums. The clean ECG is obtained without useful information lost.

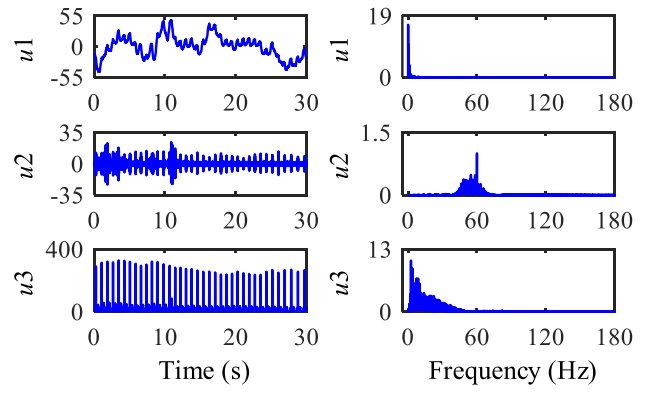


Fig. 20. Reconstructed results of VMD. The left column is the waveforms and the right column is the amplitude spectrums. More useful information is removed by two noise terms (i.e., u_1 and u_2).

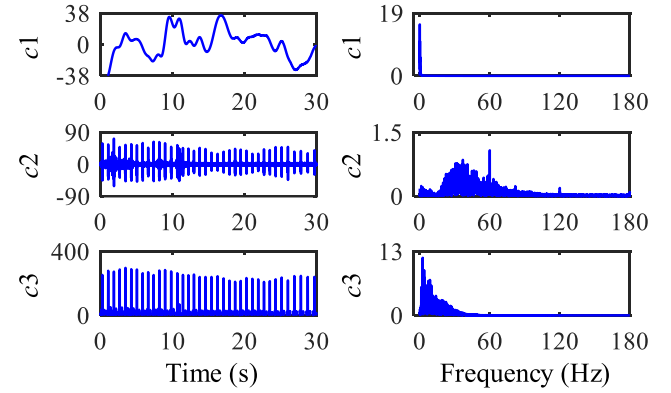


Fig. 21. Reconstructed results of CEEMD. The left column is the waveforms and the right column is the amplitude spectrums. More useful information is removed by the estimated power line interference (i.e., c_2).

60 Hz power line interference, and the clean ECG are estimated by u_1 – u_3 , respectively. Obviously, both reconstructed noise terms are affected by adjacent frequency contents. That is, more useful information is lost while noise terms are removed.

The reconstructed results of CEEMD are shown in Fig. 21. The low-frequency trend, the 60 Hz power line interference,

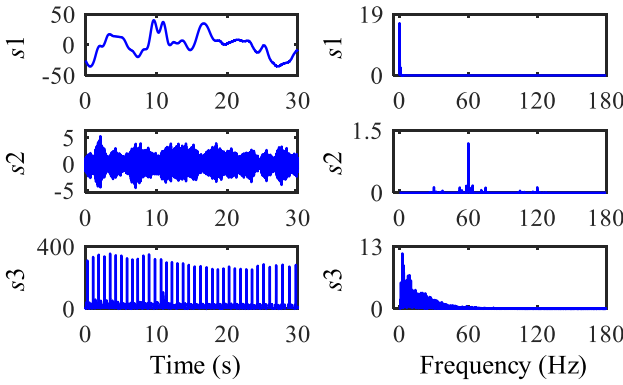


Fig. 22. Reconstructed results of WPT. The left column is the waveforms and the right column is the amplitude spectrums. A small amount of useful information is removed by the estimated power line interference (i.e., s_2).

and the clean ECG are estimated by $c1-c3$, respectively. The weak 60 Hz power line interference is mingled by adjacent frequency components. Some useful information is also eliminated by the estimated power line interference term.

The reconstructed results of WPT with the wavelet function of “db9” and the decomposition level of 8 are shown in Fig. 22. The low-frequency trend, the 60 Hz power line interference, and the clean ECG are estimated by $s1-s3$, respectively. Obviously, the weak 60 Hz power line interference is also blended by adjacent frequency contents to some extent, and a small amount of useful information is discarded by the estimated power line interference term, too.

In order to quantitatively evaluate the noise reduction effect of GVMD, the signal energy index defined by (16) is introduced. The larger the energy of denoised ECG, the more useful information is retained, the better the noise reduction effect. The energy indexes of the denoised ECGs obtained by GVMD, VMD, CEEMD, and WPT are $1.898e+7$, $1.717e+7$, $1.766e+7$, and $1.895e+7$, respectively. The most useful information is retained by GVMD. Therefore, the noise reduction effect of GVMD is the best

$$E = \sum_{n=1}^N [x(n)]^2 \quad (16)$$

where $x(n)$ is the signal, and N denotes the signal length.

To further demonstrate the noise reduction effect of GVMD, nine sets of ECG data from the MIT-BIH Arrhythmia database are analyzed, as shown in Fig. 23. The length of each analyzed ECG signal is 30 s. The noisy ECG signals are processed by GVMD, VMD, CEEMD, and WPT, respectively. The energy indexes of the denoised ECG signals by these methods are shown in Table I. Obviously, the energy indexes of denoised ECG signals obtained by GVMD are larger than those obtained by other methods. The results again demonstrate that the noise reduction effect of GVMD is superior to those of VMD, CEEMD, and WPT.

D. Discussion

The previous analysis indicates that GVMD can make full use of the feature information such as the center frequencies

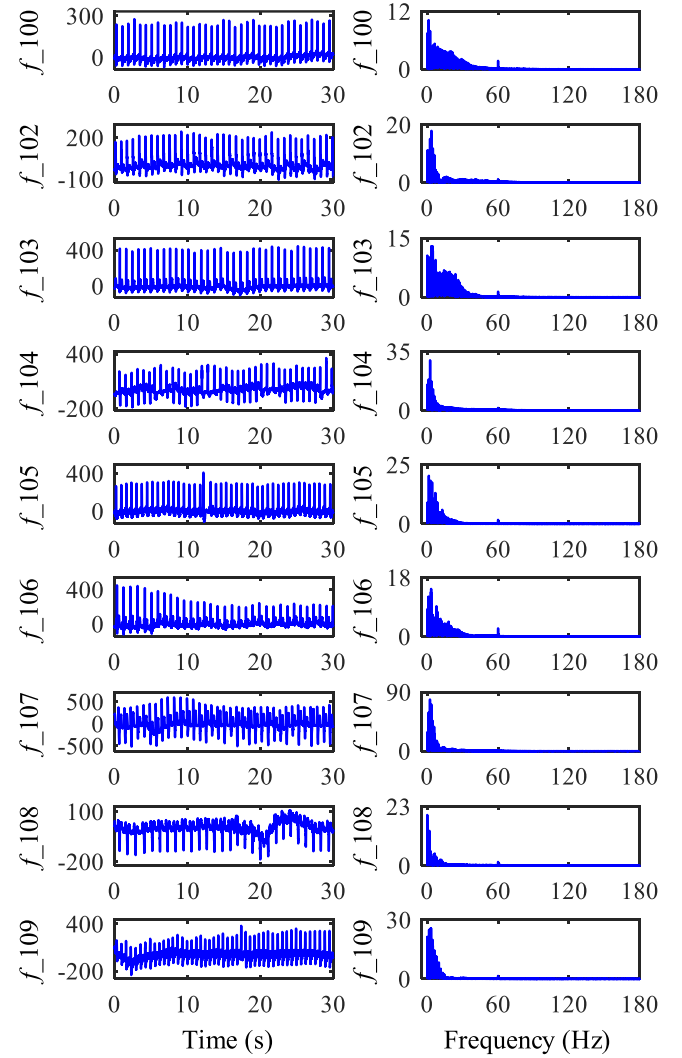


Fig. 23. Nine sets of noisy ECG signals. The left column is the waveforms and the right column is the amplitude spectrums. The original ECG signals are corrupted by low-frequency trend and weak 60 Hz power line interference.

TABLE I
ENERGY INDEXES OF DENOISED ECG SIGNALS

Data File	GVMD	VMD	CEEMD	WPT
f_{100}	$1.246e+7$	$1.089e+7$	$1.112e+7$	$1.245e+7$
f_{102}	$1.370e+7$	$1.153e+7$	$1.248e+7$	$1.317e+7$
f_{103}	$4.161e+7$	$3.872e+7$	$3.855e+7$	$4.164e+7$
f_{104}	$2.761e+7$	$2.183e+7$	$2.575e+7$	$2.662e+7$
f_{105}	$4.051e+7$	$3.597e+7$	$4.019e+7$	$4.027e+7$
f_{106}	$2.810e+7$	$2.455e+7$	$2.609e+7$	$2.756e+7$
f_{107}	$2.498e+8$	$2.220e+8$	$2.399e+8$	$2.417e+8$
f_{108}	$9.501e+6$	$7.450e+6$	$8.558e+6$	$8.552e+6$
f_{109}	$6.240e+7$	$5.508e+7$	$6.054e+7$	$6.046e+7$

and the bandwidths of signal modes to flexibly divide the frequency band and to decompose signals as required owing to the property of the multiscale and fixed-frequency decomposition. It seems that GVMD is strict with feature information of signal modes. In fact, the requirements could be met readily. The feature information can be straightforward learned about

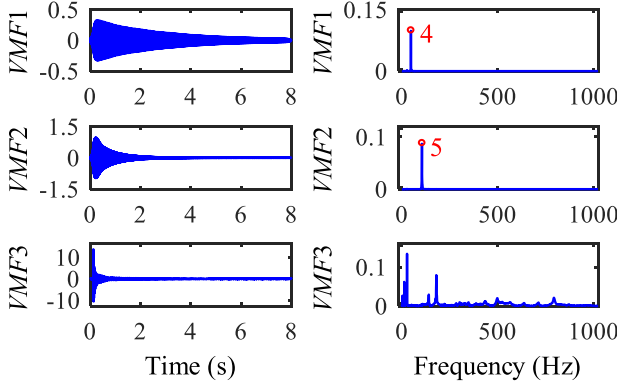


Fig. 24. Results of GVMD based on prior information. The left column is the waveforms, and the right column is the amplitude spectrums. Two sensitive modes are extracted through decomposing the original signal just into three modes through flexibly adjusting its parameters.

from the amplitude spectrum of the measured signal (see the examples in Sections III-A and III-B). The center frequency of a narrowband mode can be estimated by its peak frequency. A larger scale parameter should be set for the narrowband mode. A smaller scale parameter should be set for a wideband mode. Besides, the feature information can also be learned of based on prior knowledge (see the example in Section III-C). For another example, based on prior information, modes 4 and 5 are sensitive to the bonding defects of the explosive clad pipe (in Section III-B). The impulse response signal shown in Fig. 14 should be decomposed fewer modes to save computation time. Fig. 24 gives the analysis results of GVMD with $K = 3$, $m = 2$, $\alpha = [30000, 10000, 2]$, and $f = [47.13, 104.6, 0]$ Hz. The analysis results indicate that, unlike most signal processing methods, GVMD can flexibly make use of feature information to decompose the original signal into less modes instead of all constituent modes to meet real needs. However, how to choose an optimal scale parameter for a mode is still a problem. Shi and Yang [16] adopted the energy index to choose the parameter for VMD. We used the bandwidth index to choose the scale parameter for VMD [17]. Chen *et al.* [25] introduced the orthogonality index to adaptively choose the bandwidth parameters of ACMP. These indexes could be used to choose the optimal scale parameters for GVMD.

It is interesting that the mode of GVMD can be a narrowband mode or a wideband one owing to the property of the multiscale and fixed-frequency decomposition. And the wideband mode may be one with a slowly varying frequency (such as the FM mode in Section III-A), one with rapidly varying amplitude (such as the ECG signal in Section III-C), and one wideband mode composed of some narrowband modes or the residual signal (such as VMF8 in Fig. 15 or VMF3 in Fig. 24). Although the objective functions of the GVMD algorithm are to minimize the bandwidths, the bandwidth of each subband is governed by the scale parameter in a given situation. Owing to the property of the global data fidelity imposed by the constrained function in (2), when only a scale parameter is far smaller than other ones, the signal frequency band will be divided into several narrowband subbands and

a wideband subband or into a few narrowband subbands (see the results in Figs. 5 and 6) and a set of interlaced subbands (see the results in Fig. 7). Therefore, GVMD can decompose signals as required into a few narrowband modes or into several narrowband modes and a wideband mode (see the examples in Section III). Instead, the mode of the VMD algorithm obeys the narrowband property. The VNCMD and ACMP methods can transform a wideband chirp mode into a narrowband one via demodulation techniques. Therefore, the modes of VNCMD and ACMP can be narrowband ones or wideband chirp ones but cannot be wideband ones with quickly varying amplitude [24]–[26]. Therefore, GVMD is different from VNCMD and ACMP. In order to further verify the effectiveness of GVMD to analyze the signal containing a wideband mode with the time-varying amplitude. The simulated signal is designed as follows:

$$\begin{cases} x(t) = \cos(40\pi t) + 0.4 \cos(80\pi t) + \sum_j p_j(t - jT) \\ p(t) = e^{-48\pi t} \sin(2400\pi t). \end{cases} \quad (17)$$

The simulated signal is composed of two harmonic modes and a periodic free decay oscillation mode with the time period being 0.05 s. The periodic free decay oscillation mode is a wideband one with rapidly varying amplitude, which is often used to model the impact vibration of the equipment. Fig. 25 provides the analysis results of GVMD and ACMP. GVMD can well separate three constituent modes and adaptively identify the periodic free decay mode with rapidly varying amplitude as a wideband mode. ACMP decomposes the simulated signal into two low-frequency modes and 27 higher frequency modes. The periodic free decay oscillation mode with rapidly varying amplitude is not identified straightforward as a wideband mode but multiple narrowband modes by ACMP, which needs to be reconstructed by 27 higher frequency modes. The estimated errors of GVMD to 20 and 40 Hz harmonic modes and the periodic free decay oscillation mode, which are computed by (15), are 0.0770, 0.1896, and 0.0772, respectively. The estimated errors of ACMP to three modes are 0.0806, 0.1981, and 0.3654, respectively. Obviously, the estimated errors of three modes obtained by GVMD are smaller. Similarly, if the wideband ECG signal with rapidly varying amplitude were analyzed by ACMP, it would be decomposed into numerous narrowband modes. To save space, the analysis results are omitted.

However, the original signal contains more than one wideband mode. If they are overlapped or interlaced in the frequency domain, they will not be well identified as wideband modes anymore by GVMD. For the interlaced and wide-banded modes, they could be reconstructed after being decomposed into multiple narrowband modes. For the wideband modes which are overlapped in the frequency domain but well separate in the time-frequency domain, they will be mistakenly separated by GVMD. Just as does in VNCMD and ACMP, solving the models of GVMD in the time-frequency domain may be a good idea.

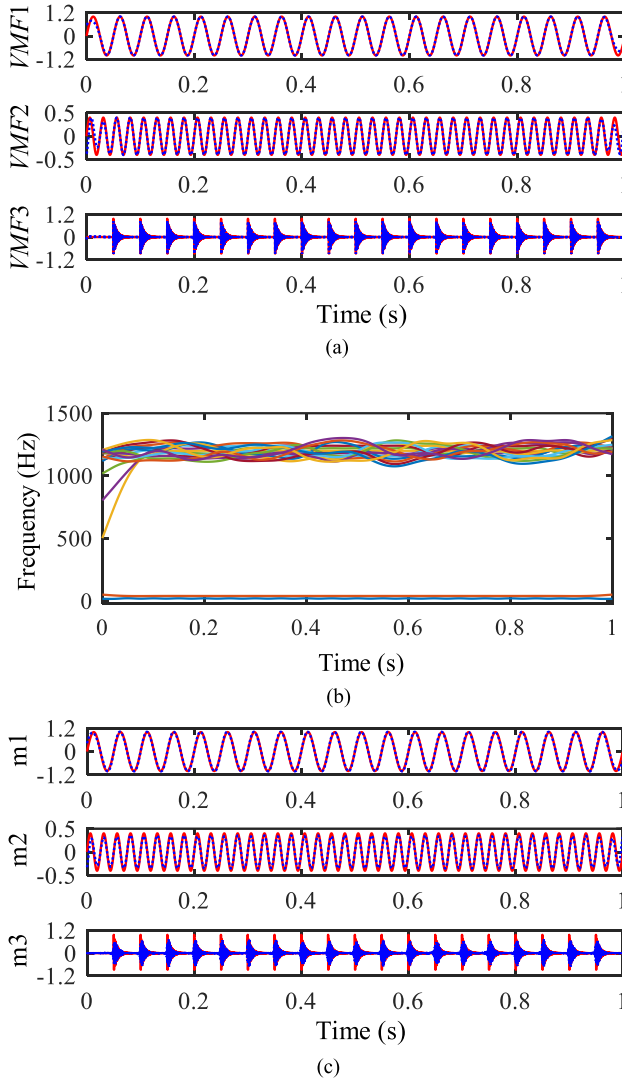


Fig. 25. Results of GVMD and ACMP. GVMD can well separate two narrowband harmonic modes and the wideband periodic free decay mode. Instead, ACMP can well separate two narrowband harmonic modes but not the wideband periodic free decay mode straightforward, which needs to be reconstructed by multiple narrowband modes. (a) Results of GVMD with $\alpha = [5000, 6000, 20]$, $f = [20, 40, 0]$ Hz, $K = 3$, and $m = 2$. (b) Estimated instantaneous frequencies by ACMP. (c) Analysis results of ACMP.

IV. CONCLUSION

In this article, the mathematical theory on how to construct and solve the models is completed to lay a foundation for the newly proposed algorithm called GVMD, which can decompose the input signal into several narrowband modes or a few narrowband modes and a wideband mode as required while obtaining the corresponding center frequencies. In the proposed models, individual constrained optimization problem is constructed for each component so as to highlight the local characteristics of the signal while considering the global data fidelity. The proposed models are solved by modified ADMM to realize the multiscale and fixed-frequency decomposition. In the proposed model, the core assumption is that modes are not overlapped in the frequency domain.

The frequency band division manner of GVMD is studied by the Dirac pulse signal. The frequency band can be divided as required through flexibly adjusting the spectrum positions

and frequency scales. The spectrum positions of GVMD can be specified by the prior center frequencies. The frequency scales of GVMD are influenced by the scale parameters, and smaller frequency scales can be gained with larger scale parameters in the given situation.

The effectiveness of GVMD is verified on simulated and real signals. The results indicate that compared with the methods such as CEEMD, WPT, VMD, and ACMP, GVMD can decompose original signals as required through making use of feature information to effectively obtain the desired modes.

The parameters of GVMD, such as prior center frequencies and scale parameters, can be flexibly defined based on feature information. However, the frequency scales of GVMD are influenced by multiple factors. In the given situations, the frequency scales can be flexibly adjusted by scale parameters. How to select the optimal scale parameters will be studied in the future.

REFERENCES

- [1] K. Dragomiretskiy and D. Zosso, "Variational mode decomposition," *IEEE Trans. Signal Process.*, vol. 62, no. 3, pp. 531–544, Feb. 2014.
- [2] J. Giles, "Empirical wavelet transform," *IEEE Trans. Signal Process.*, vol. 61, no. 16, pp. 3999–4010, Aug. 2013.
- [3] N. E. Huang *et al.*, "The empirical mode decomposition and the Hilbert spectrum for nonlinear and non-stationary time series analysis," *Proc. Roy. Soc. London. A, Math., Phys. Eng. Sci.*, vol. 454, no. 1971, pp. 903–995, Mar. 1998.
- [4] Z. Wu and N. E. Huang, "Ensemble empirical mode decomposition: A noise-assisted data analysis method," *Adv. Adapt. Data Anal.*, vol. 1, no. 1, pp. 1–41, Jan. 2009.
- [5] J.-R. Yeh, J.-S. Shieh, and N. E. Huang, "Complementary ensemble empirical mode decomposition: A novel noise enhanced data analysis method," *Adv. Adapt. Data Anal.*, vol. 2, no. 2, pp. 135–156, Apr. 2010.
- [6] C. Zhang and Y. Liu, "A two-step denoising strategy for early-stage fault diagnosis of rolling bearings," *IEEE Trans. Instrum. Meas.*, vol. 69, no. 9, pp. 6250–6261, Sep. 2020.
- [7] Y. Xu, Y. Deng, J. Zhao, W. Tian, and C. Ma, "A novel rolling bearing fault diagnosis method based on empirical wavelet transform and spectral trend," *IEEE Trans. Instrum. Meas.*, vol. 69, no. 6, pp. 2891–2904, Jun. 2020.
- [8] A.-O. Boudraa and J.-C. Cexus, "EMD-based signal filtering," *IEEE Trans. Instrum. Meas.*, vol. 56, no. 6, pp. 2196–2202, Dec. 2007.
- [9] K. Hong, L. Wang, and S. Xu, "A variational mode decomposition approach for degradation assessment of power transformer windings," *IEEE Trans. Instrum. Meas.*, vol. 68, no. 4, pp. 1221–1229, Apr. 2019.
- [10] G. Tang, Y. Wang, Y. Huang, N. Liu, and J. He, "Compound bearing fault detection under varying speed conditions with virtual multichannel signals in angle domain," *IEEE Trans. Instrum. Meas.*, vol. 69, no. 8, pp. 5535–5545, Aug. 2020.
- [11] M. Mishra, S. Banerjee, D. C. Thomas, S. Dutta, and A. Mukherjee, "Detection of third heart sound using variational mode decomposition," *IEEE Trans. Instrum. Meas.*, vol. 67, no. 7, pp. 1713–1721, Jul. 2018.
- [12] Y. Wang, R. Markert, J. Xiang, and W. Zheng, "Research on variational mode decomposition and its application in detecting rub-impact fault of the rotor system," *Mech. Syst. Signal Process.*, vols. 60–61, pp. 243–251, Aug. 2015.
- [13] Z. Li, J. Chen, Y. Zi, and J. Pan, "Independence-oriented VMD to identify fault feature for wheel set bearing fault diagnosis of high speed locomotive," *Mech. Syst. Signal Process.*, vol. 85, pp. 512–529, Feb. 2017.
- [14] D. Zhang and Z. Feng, "Application of variational mode decomposition based demodulation analysis in gearbox fault diagnosis," in *Proc. IEEE Int. Instrum. Meas. Technol. Conf.*, Taipei, Taiwan, May 2016, pp. 1–6, doi: 10.1109/I2MTC.2016.7520586.
- [15] X. An and J. Yang, "Denoising of hydropower unit vibration signal based on variational mode decomposition and approximate entropy," *Trans. Inst. Meas. Control*, vol. 38, no. 3, pp. 282–292, Mar. 2016.

- [16] P. Shi and W. Yang, "Precise feature extraction from wind turbine condition monitoring signals by using optimised variational mode decomposition," *IET Renew. Power Gener.*, vol. 11, no. 3, pp. 245–252, Feb. 2017.
- [17] Y. Guo, Z. Zhang, J. Cao, T. Gong, and W. Yang, "An optimized variational mode decomposition for extracting weak feature of viscoelastic sandwich cylindrical structures," *Meas. Sci. Technol.*, vol. 29, no. 3, Mar. 2018, Art. no. 035006.
- [18] W. Yang, Z. Peng, K. Wei, P. Shi, and W. Tian, "Superiorities of variational mode decomposition over empirical mode decomposition particularly in time–frequency feature extraction and wind turbine condition monitoring," *IET Renew. Power Gener.*, vol. 11, no. 4, pp. 443–452, 2017.
- [19] Z. Gao, X. Wang, J. Lin, and Y. Liao, "Online evaluation of metal burn degrees based on acoustic emission and variational mode decomposition," *Measurement*, vol. 103, pp. 302–310, Jun. 2017.
- [20] Y. Wang and R. Markert, "Filter bank property of variational mode decomposition and its applications," *Signal Process.*, vol. 120, pp. 509–521, Mar. 2016.
- [21] S. I. McNeill, "Decomposing a signal into short-time narrow-banded modes," *J. Sound Vib.*, vol. 373, pp. 325–339, Jul. 2016.
- [22] Y. Guo, Z. Zhang, T. Gong, J. Cao, and W. Yang, "Generalized variational mode decomposition for interlayer slipping detection of viscoelastic sandwich cylindrical structures," *Meas. Sci. Technol.*, vol. 29, no. 9, Sep. 2018, Art. no. 095001.
- [23] N. Mohan, K. S. Sachin, P. Poornachandran, and K. P. Somam, "Modified variational mode decomposition for power line interference removal in ECG signals," *Int. J. Electr. Comput. Eng.*, vol. 6, no. 1, pp. 151–159, 2016.
- [24] S. Chen, X. Dong, Z. Peng, W. Zhang, and G. Meng, "Nonlinear chirp mode decomposition: A variational method," *IEEE Trans. Signal Process.*, vol. 65, no. 22, pp. 6024–6037, Nov. 2017.
- [25] S. Chen, Y. Yang, Z. Peng, X. Dong, W. Zhang, and G. Meng, "Adaptive chirp mode pursuit: Algorithm and applications," *Mech. Syst. Signal Process.*, vol. 116, pp. 566–584, Feb. 2019.
- [26] S. Chen, Y. Yang, Z. Peng, S. Wang, W. Zhang, and X. Chen, "Detection of rub-impact fault for rotor-stator systems: A novel method based on adaptive chirp mode decomposition," *J. Sound Vib.*, vol. 440, pp. 83–99, Feb. 2019.
- [27] S. Boyd, "Distributed optimization and statistical learning via the alternating direction method of multipliers," *Found. Trends Mach. Learn.*, vol. 3, no. 1, pp. 1–122, 2010.
- [28] Y. Si, Z. Zhang, Q. Liu, W. Cheng, and F. Yuan, "Detecting the bonding state of explosive welding structures based on EEMD and sensitive IMF time entropy," *Smart Mater. Struct.*, vol. 23, no. 7, Jul. 2014, Art. no. 075010.
- [29] G. B. Moody and R. G. Mark, "The impact of the MIT-BIH arrhythmia database," *IEEE Eng. Med. Biol. Mag.*, vol. 20, no. 3, pp. 45–50, May/Jun. 2001. [Online]. Available: <http://physionet.org/physiobank/database/mitdb/>



Yanfei Guo received the M.Sc. degree in electrical engineering from Henan Polytechnic University, Jiaozuo, China, in 2006, and the Ph.D. degree in mechanical engineering from Xi'an Jiaotong University, Xi'an, China, in 2020.

He is currently a Lecturer with the School of Electronics and Information Engineering, Taiyuan University of Science and Technology, Taiyuan, China. His research interests include signal processing and fault diagnosis.



Zhousuo Zhang received the M.Sc. and Ph.D. degrees in mechanical engineering from Xi'an Jiaotong University, Xi'an, China, in 1991 and 2004, respectively.

He is currently a Professor with the School of Mechanical Engineering, Xi'an Jiaotong University. His research interests include condition monitoring and fault diagnosis of mechanical equipment, failure prediction and life prediction of equipment, and structure dynamic analysis and state detection.